The role of gene dosage in budding yeast centrosome scaling and spontaneous diploidization

Jingjing Chen*, Zhiyong Xiong*[§], Danny E. Miller*[#], Zulin Yu*, Scott McCroskey*, William D. Bradford*, Ann M. Cavanaugh*[†] and Sue L. Jaspersen*[‡]

*Stowers Institute for Medical Research, Kansas City, Missouri 64110

[‡]Department of Molecular and Integrative Physiology, University of Kansas Medical Center, Kansas City, Kansas 66160

Running Title: Centrosome scaling and diploidization

Corresponding author:
Sue L. Jaspersen
Stowers Institute for Medical Research
1000 E. 50th Street
Kansas City, MO 64110
Phone: 816-926-4325
E-mail: slj@stowers.org

[§] Current address: Inner Mongolia Potato Engineering and Technology Research Centre, Inner Mongolia University, Hohhot, Inner Mongolia 010021 China

[#] Current address: Department of Pediatrics, Division of Genetic Medicine, University of Washington and Seattle Children's Hospital, Seattle, WA, 98105

[†] Current address: Department of Biology, Creighton University, Omaha, NE 68178

Abstract

Ploidy is the number of whole sets of chromosomes in a species. Ploidy is typically a stable cellular feature that is critical for survival. Polyploidization is a route recognized to increase gene dosage, improve fitness under stressful conditions and promote evolutionary diversity. However, the mechanism of regulation and maintenance of ploidy is not well characterized. Here, we examine the spontaneous diploidization associated with mutations in components of the *Saccharomyces cerevisiae* centrosome, known as the spindle pole body (SPB). Although SPB mutants are associated with defects in spindle formation, we show that two copies of the mutant in a haploid yeast favors diploidization in some cases, leading us to speculate that the increased gene dosage in diploids 'rescues' SPB duplication defects, allowing cells to successfully propagate with a stable diploid karyotype. This copy number-based rescue is linked to SPB scaling: certain SPB subcomplexes do not scale or only minimally scale with ploidy. We hypothesize that acquisition of lesions in structures with incompatible allometries such as the centrosome may drive changes such as whole genome duplication, which have shaped the evolutionary landscape of many eukaryotes.

Author Summary

Ploidy is the number of whole sets of chromosomes in a species. Most eukaryotes alternate between a diploid (two copy) and haploid (one copy) state during their life and sexual cycle. However, as part of normal human development, specific tissues increase their DNA content. This gain of entire sets of chromosomes is known as polyploidization, and it is observed in invertebrates, plants and fungi, as well. Polyploidy is thought to improve fitness under stressful conditions and promote evolutionary diversity, but how ploidy is determined is poorly understood. Here, we use budding yeast to investigate mechanisms underlying the ploidy of wild-type cells and specific mutants that affect the centrosome, a conserved structure involved in chromosome segregation during cell division. Our work suggests that different scaling relationships (allometry) between the genome and cellular structures underlies alterations in ploidy. Furthermore, mutations in cellular structures with incompatible allometric relationships with the genome may drive genomic changes such duplications, which are underly the evolution of many species including both yeasts and humans.

Introduction

Multiple conserved processes act together to ensure eukaryotic cells maintain a stable chromosome composition, called the karyotype. Most organisms have a diploid karyotype with two copies of each chromosome (Ezov et al. 2006). In nature, fungi are also commonly diploids, however, a haploid karyotype can be stably maintained in most lab strains (Gerstein and Otto 2009; Herskowitz 1988). Changes in the karyotype through gains or losses of one or more chromosomes leads to aneuploidy, which is associated with miscarriage, cancer and fungal drug resistance (Gianaroli et al. 1999; Storchova and Pellman 2004; Selmecki, Forche, and Berman 2006; Gordon, Resio, and Pellman 2012). Gains of whole sets of chromosomes (polyploidy) is another type of karyotype alteration that has driven evolution of many eukaryotes, including vertebrates and yeast such as *Saccharomyces cerevisiae* (Lee, Davidson, and Duronio 2009; Selmecki et al. 2015; Mittal et al. 2017; Otto 2007; Harari et al. 2018). Increased ploidy is observed in certain highly differentiated human tissues such as liver parenchyma, heart muscle, placenta and bone marrow (Anatskaya and Vinogradov 2007; Liu et al. 2010; Orr-Weaver 2015), and it is frequently observed in plants (Soltis et al. 2015). However, polyploidy is also linked to aneuploidy as increased ploidy often leads to chromosome instability (CIN) (Amend et al. 2019; Storchova and Pellman 2004; Kops, Weaver, and Cleveland 2005; Fujiwara et al. 2005; Mayer and Aguilera 1990). For example, in budding yeast the rate of chromosome loss in triploids and tetraploids is 30- and 1000-fold higher than haploids (Andalis et al. 2004). The mechanism(s) resulting in CIN in polyploids are poorly understood but may be linked to incompatible allometries (biological scaling relationships) driven by increasing genome size (Varberg and Jaspersen 2018; Hara and Kimura 2011; Storchova et al. 2006; Andalis et al. 2004).

The cell division cycle is a highly conserved process that ensures chromosomes are replicated and segregated into daughter cells. Throughout eukaryotes, chromosomes are distributed into daughter cells by the mitotic spindle, a microtubule network formed around two spindle poles known as centrosomes in metazoans or spindle pole bodies (SPBs) in fungi. Duplication of the centrosome/SPB is coupled with the cell cycle such that cells entering mitosis have exactly two spindle poles to form a bipolar spindle (Ruthnick and Schiebel 2018; Cavanaugh and Jaspersen 2017). Errors in centrosome duplication result in the formation of monopolar or multipolar spindles. This has long been considered a driving factor in aneuploidy and polyploidy despite mechanisms to cluster multipolar spindles or surveillance mechanisms to detect spindle defects (Vitre and Cleveland 2012). In *Saccharomyces cerevisiae* a mutant defective in SPB duplication was isolated by Lee Hartwell in his famous screen for cell division cycle mutants (Hartwell et al. 1973). *cdc31-1* (allelic to *cdc31-2* used here) mutants arrest in metaphase due to monopolar spindles. Although the mutant was isolated in a yeast with a haploid karyotype, *cdc31-1* cells were found to be polyploid (diploid) (Schild, Ananthaswamy, and Mortimer 1981). This phenotype of spontaneous diploidization is not unique to *cdc31-1,* also having been described for other SPB components and regulators (Sing et al. 2018; Jaspersen, Giddings, and Winey 2002; Jaspersen et al. 2006; Chen et al. 2019; Kupke et al. 2011; Vallen et al. 1994; Winey et al. 1991; Chial et al. 1999).

In the electron microscope, the SPB appears as a trilaminar plaque-like structure embedded in the nuclear membrane (Byers and Goetsch 1974). Associated with one side is a specialized region of the nuclear envelope known as the half-bridge. Molecularly, the ~1 GDa SPB is composed of 18 components present in multiple copies. Each protein localizes to a distinct region in the SPB, including the core, the half-bridge

or the membrane region that anchors the SPB to the nuclear envelope (referred to here as the SPB luminal ring) (Cavanaugh and Jaspersen 2017; Ruthnick and Schiebel 2018). The half-bridge plays an essential role in SPB duplication while the ultimate function of the core is microtubule nucleation.

Polyploidy may result from errors in chromosome segregation, but, somewhat paradoxically, increases in ploidy expand the burden of chromosomes that must be replicated and segregated by the cell cycle machinery. While polyploidy does not lead to the proteotoxic stress observed in many aneuploids (Sheltzer and Amon 2011; Oromendia and Amon 2014), genetic analysis of haploid, diploid and tetraploid yeast cells pointed to three processes that are essential for genome stability in cells of higher ploidy (tetraploids) but non-essential in cells of lower ploidy (haploids and diploids): homologous recombination, sister chromatid cohesion and mitotic spindle function (Storchova et al. 2006; Storchova 2014). In yeast, where a single microtubule binds to each chromosome via its kinetochore (Joglekar et al. 2006), the number of microtubules must scale with ploidy. Consistent with this idea, the size of the SPB core, measured by electron microscopy (EM) as the diameter across its central region, increases linearly with ploidy: from 90-110 nm in haploids, to 160 nm in diploids and 240 nm in tetraploids (Adams and Kilmartin 1999; Kilmartin 2003; Byers and Goetsch 1974). How the SPB scales in size is unknown. The simplest idea, that polyploids have extra copies of SPB genes, seems insufficient as the SPB of haploid cells can also scale in size when the cell cycle is delayed or when the number of centromeres is increased (Winey et al. 1993; Nannas et al. 2014). In addition, in SPB mutants that spontaneously diploidize, the cell must build a larger SPB and nucleate more microtubules – so it is unclear why the mutation would not result in another error in segregation that would further increase ploidy.

In metazoans, centrosome size also correlates with spindle size, and changes in its size have been linked to defects in chromosome segregation, aneuploidy and cancer (Vitre and Cleveland 2012; Cabral et al. 2019; Marshall 2011; Marteil et al. 2018). Here, we used budding yeast as a model system to examine the relationship between ploidy changes and SPB size scaling at a molecular level. We examined the polyploidy associated with SPB mutants and performed a genetic screen to isolate suppressors of *cdc31-2* diploidization. We found that spontaneous diploidization rescues the growth defect associated with some, but not all, SPB mutants. Our data shows that mutations that are rescued by increased ploidy are only found in genes encoding specific SPB components that localize to regions of the SPB structure that we show do not scale linearly with chromosome number. We propose that polyploidy acts as a 'dosage' suppressor and that acquisition of malfunctional centrosomes could drive eukaryotic evolution or disease progression by promoting changes such as whole genome duplication.

Results

Spontaneous diploidization in SPB mutants

Cdc31 is the yeast centrin ortholog, a small, highly conserved calcium binding protein present at centrosomes and other microtubule-organizing centers (MTOCs) across eukaryotes. A temperature-sensitive mutation in *cdc31-2* (E133K) causes haploid yeast cells to undergo spontaneous diploidization at the permissive growth temperature (23°C) immediately upon loss of a wild-type copy of *CDC31*, a phenotype we will refer to as increase-in-ploidy (IPL) (Chan and Botstein 1993). The IPL phenotype is observed by flow cytometry as 2N and 4N peaks compared to the 1N and 2N peaks seen in haploid cells (Figure 1A). Whole genome sequencing (WGS) of *cdc31-2* mutants shows that the IPL is an example of autopolyploidy, with two exact copies of each chromosome (diploid control in Figure 2D, Table S1). Examination of spindle structure by fluorescence microscopy showed that 59% of *cdc31-2* large budded cells contained a bipolar spindle (Figure 1A). Interestingly, we did not observe evidence of *cdc31-2* progressing to tetraploids, suggesting that these mutants are maintained as stable diploids with fully compensated microtubule nucleation ability as a result of their IPL phenotype. Together, these results show that loss of Cdc31 function at 23°C can be overcome by spontaneous transition to a diploid state.

It is unclear why the mutant cells are able to divide as stable diploids without forming tetraploids. One possibility is that tetraploids do indeed form but are quickly reverted to diploids through chromosome loss although the perfect ploidy of the *cdc31-2* diploids argues against this possibility. The IPL phenotype of *cdc31-2* and other mutants is thought to arise from a monopolar cell division in haploids, resulting in an aploid cell that dies and a diploid cell that is able to undergo successful divisions as a diploid (Jaspersen, Giddings, and Winey 2002; Sing et al. 2018). Additionally, acquisition of

suppressor mutation that bypasses the SPB defect caused by the original mutation may be involved in diploidization (Figure 1B).

Suppressors of cdc31-2 spontaneous diploidization

To determine the mechanisms that drive the *cdc31-2* IPL phenotype and prevent further increases in ploidy, we developed a forward genetic screen to identify suppressors of the spontaneous diploidization observed in *cdc31-2* mutants (Figure 2A). Because *cdc31-2* is a recessive mutation, we maintained cells as haploids using a plasmid containing a wild-type copy of *CDC31* (*pURA3-CDC31*), known as a covering or complementing plasmid. Haploid *MATα cdc31-2 pURA3-CDC31* cells were mutagenized with ethyl methanesulfonate (EMS), individual mutagenized cells were selected, and the covering plasmid then was removed by growth on 5-fluoroorotic acid (5-FOA). Cells that contain an IPL suppressor are haploid while the remainder spontaneously diploidize due to the *cdc31-2* allele that is uncovered following plasmid loss (Figure 2A).

In budding yeast, the ability to sexually reproduce is not controlled by chromosome number but rather by the mating type locus (MAT) present on chromosome III. Typical diploids are heterozygous for MAT (*MATa/MATα*) and are therefore able to undergo meiosis to produce four viable haploid progeny known as spores. Triploid meiosis (*MATa/MATa/MATα* or *MATa/MATα/MATα*) is catastrophic because few spores contain chromosome combinations compatible with life. In our strain background, the viability of meiotic progeny from diploid meiosis in yeast homozygous for *cdc31-2* is 88.2% while the viability of progeny from triploids is 6.2% (Figure 2B). We therefore screened for suppressors of IPL through a selection scheme involving a non-mutagenized *MATa cdc31-2 pURA3-CDC31* strain mated with the EMS-induced mutant library. In this system, only *cdc31-2* cells that contain a suppressor of spontaneous diploidization will

mate to form diploids, undergo a successful meiosis and generate viable progeny. In contrast, cells that spontaneously diploidized will mate to form triploids, which will die under the meiotic selection conditions (Figure 2B).

Of ~100,000 EMS mutagenized cells that were screened as described, we isolated 61 possible suppressors of the *cdc31-2* IPL phenotype (Figure 2C). To confirm that these cells had suppressed diploidization, we performed flow cytometry on all 61 hits. Of these, 54 displayed predominately 1N and 2N peaks characteristic of haploid cells and these were pursued further. Our system utilizes selection with 5-FOA, which is converted into a toxic metabolite in yeast containing *URA3* (Boeke et al. 1987). If a mutation is introduced into the *URA3* gene by EMS, haploid *cdc31-2* cells containing the covering plasmid would be able to grow on this counter-selection. To remove these potential false positives, we tested our 54 potential suppressors and found that 43 retained the covering plasmid. Further evaluation of these remaining 11 suppressor strains showed that each was linked to a single locus in the nuclear genome. Suppression of the *cdc31-2* IPL in one tetrad is shown in Figure 2C.

From these eleven suppressors, we chose three for further characterization by Illumina sequencing. Pooled genomic DNA from 20 meiotic progeny with and without the suppressor was analyzed. No single nucleotide or insertion/deletion polymorphisms were shared among all three strains, suggesting that suppression was not caused by a change in a single gene shared by all three mutants (Table S1). An obvious suppressor mutation within the genome also was not obvious. Strikingly, all three suppressors showed increased read depth for the entire length of chromosome XV relative to control when compared to all other chromosomes (Figure 2D). Thus, all three suppressors of

230 *cdc31-2* IPL contained two complete copies of chromosome XV while retaining a single
231 copy of all other chromosomes.
232
233 Using a quantitative PCR assay (Wang et al. 2002), we determined that the increased
234 copy number for chromosome XV was present in all eleven isolated suppressors (Figure
235 2E). Most contained a single copy of chromosomes I-XIV and chromosome XVI,
236 however, one (*ems5*) had a more complex karyotype that may be due chromosome
237 rearrangements such as diploidization followed by chromosome loss (Figure 2E).
238 Alternatively, this mutant may exhibit cell to cell variation in chromosome content.
239 Because all cells contained two copies of chromosome XV, this phenotype was further
240 characterized as it suggests that disomy for chromosome XV can suppresses IPL of
241 *cdc31-2*.
242
243 *Increased cdc31-2 dosage suppresses diploidization*
244 Cells disomic for chromosome XV exhibit a number of phenotypes, including a short
245 delay in G1 phase of the cell cycle and a small increase in cell volume compared to
246 normal haploid cells (Torres et al. 2007; Torres et al. 2010; Bonney, Moriya, and Amon
247 2015). However, these phenotypes seem unlikely to be related to the mechanism of
248 *cdc31-2* suppression since we did not recover disomies for other chromosomes with
249 similar effects on cell size and the cell cycle, nor did they suppress *cdc31-2* IPL when
250 directly tested. The specificity for chromosome XV suggests that suppression is linked to
251 a gene or genes located on that chromosome, which are known to be upregulated in
252 disomic strains relative to the rest of the haploid genome (Mulla, Zhu, and Li 2014). It
253 seems likely that doubling the dosage of the gene(s) on chromosome XV is sufficient to
254 alleviate the defect in SPB duplication that occurs in haploid *cdc31-2* mutants.

Importantly, the *CDC31* locus is located on the right arm of chromosome XV, making *cdc31-2* itself a leading candidate for dosage-mediated suppression.

To test the idea that *cdc31-2* itself suppresses IPL, we first tested if *cdc31-2* was necessary for suppression in the disomic strain (*cdc31-2 2xChXV*) (Figure 3A). Deletion of one copy of *cdc31-2* (*cdc31-2 2xChXV(cdc31Δ::KANMX)*) reduced growth at 23°C compared to the disomic control to a level similar to *cdc31-2* mutants (Figure 3A, C). These cells also spontaneously diploidized like *cdc31-2* (Figure 3B). Thus, it appears that the *cdc31-2* locus is necessary for suppression of IPL in the disomic strain.

To test if an extra single copy of *cdc31-2* is sufficient to suppress IPL, we integrated a single copy of *cdc31-2* containing its endogenous promoter, terminator and coding sequence into a covered haploid *cdc31-2* strain at the *HIS3* locus on chromosome XV (Figure 3D). We also constructed isogenic strains containing an empty vector or wild-type *CDC31* at *HIS3* as controls (Figure 3D). As shown in Figure 3E, a single extra copy of *cdc31-2* integrated into the genome in combination with *cdc31-2* at the genomic locus (*cdc31-2 his3::cdc31-2-HIS3*) is sufficient to suppress IPL observed in *cdc31-2* mutants after removal of the covering plasmid on 5-FOA. These cells grow as well, or better, than *cdc31-2* mutants that spontaneously diploidize or *cdc31-2* carrying a chromosome XV disome (Figure 3C & F). This could be due the fact that a single gene rather than multiple genes is altered, resulting in little or no changes in the overall cellular proteome. Despite increased growth at 23°C and 30°C, two copies of *cdc31-2* are unable to suppress temperature sensitivity at 37°C (Figure 3C & F). This finding suggests that the copy number-based suppression of IPL at 23°C occurs via a different mechanism than dosage suppression of *cdc31^{ts}* alleles at 37°C, which is probably based on bypassing, stabilizing or upregulating the mutant protein.

281

282 *SPB scaling along with ploidy change*

283 One effect of polyploidy is an increase in the size of intracellular structures. Based on
284 EM analysis of SPB structure, SPB diameter (measured at the SPB core) increases from
285 110 nm in haploid cells to 160 nm in diploids; however, SPB height does not change
286 (Byers and Goetsch 1974) (Figure 4A-B). The length of the half-bridge also does not
287 change when ploidy is increased, and its width may only marginally increase (Figure
288 4B). One possibility linking spontaneous diploidization to a subset of SPB mutants such
289 as *cdc31-2* is based on 'dosage suppression' – diploids have two gene copies, and
290 presumably twice the amount of protein, to make the same structure that is needed in
291 both haploids and diploids. For other SPB mutants, diploidization would not have the
292 same effect as a larger structure requiring more protein is built.

293

294 A rigorous test of this idea involves the comparison of protein levels at the SPB for
295 different components. If our hypothesis is correct, levels of core proteins will be higher
296 in diploids compared to haploids, as the size of the core, in theory, scales approximately
297 two-fold between haploids and diploids. Alternatively, a similar increase in ploidy should
298 not affect levels of half-bridge proteins since its size is thought to be similar in haploids
299 and diploids (Kilmartin 2003). We anticipated that levels of the luminal ring would also
300 increase in size in diploids, although given the differences in geometry and organization
301 the luminal ring may not increase to the same extent as the core (Figure 4B). To directly
302 test these hypotheses, we compared the intensity of multiple SPB components
303 endogenously-tagged with mTurquoise2 at the C-terminus in both haploid and
304 homozygous diploid strains, with the exception of Kar1, which was tagged at the N-
305 terminus. We were unable to functionally tag Cdc31, similar to previous reports (Yoder et
306 al. 2003; Jaspersen, Giddings, and Winey 2002; Kilmartin 2003). SPB components

clustered into three groups based on the intensity increase observed in diploids: no/mild (up to 1.1-fold), modest (1.1-1.4-fold) and major (over 1.4-fold) increase. Somewhat unexpectedly, none showed the anticipated increased fluorescence intensity based on scaling models and EM measurements (Figure 4C). For example, core SPB components (Spc110, Spc29, Tub4, Spc42), which underwent major scaling, showed a ~1.4-1.5-fold increase in diploids.

The group that showed a mild increase in diploids contained components of the luminal ring: Nbp1, Bbp1 and Mps2 (Figure 4C). The observation that this SPB substructure does not scale as predicted in our theoretical model could be caused by heterogeneity in ring shape (Chen et al. 2019) or by a difference in the actual mechanism of ring expansion. During post-mitotic nuclear pore complex (NPC) assembly, the membrane ring expands through a process known as radial dilation (Shahin et al. 2005; Otsuka et al. 2018). A constant total amount of protein is spread over an expanding NPC core, decreasing protein area with the increase in size. Our data suggests that the luminal ring expands by a similar radial dilation process (Figure 4C).

The levels of half-bridge proteins Sfi1 and Kar1 showed a modest increase in diploids (Figure 4C). This suggests that the width of the bridge scales a small amount from haploids to diploids. Mps3 also showed an increase; as a dual component of the half-bridge and the luminal ring (Chen et al. 2019), this is consistent with bridge scaling (as seen for Sfi1 and Kar1) and radial dilation (as seen for Nbp1, Bbp1 and Mps2). Although we were unable to visualize Cdc31 microscopically, we found that an extra copy of *CDC31* resulted in a 50% increase in total Cdc31 levels, measured by western blotting of whole cell extracts (Figure 4D). As Cdc31 is present at multiple structures throughout the cell (Fischer et al. 2004; Chen and Madura 2008; Myers and Payne 2017), this would

likely reflect a moderate increase in its levels at the SPB, similar to the trend we observed for the other half-bridge components, Sfi1, Kar1 and Mps3. Overall, our data are consistent with the idea that IPL may be linked to scaling of the SPB.

Gene dosage as a general mechanism to suppress IPL in SPB mutants

Diploidization is not unique to *cdc31-2*, but it is also observed in other SPB mutants, including some, but not, all alleles of *MPS3*, *KAR1*, *NBP1* and *MPS2* (Table 1). The fact that the phenotype is limited to half-bridge and luminal ring SPB components may be due in part to the fact that these SPB substructures do not or only modestly scale in size (Figure 4B-C). However, the observation that it is limited to certain specific alleles suggests the dosage-dependent IPL mechanism also involves the mutant protein and its role at the SPB. For example, a common defect in SPB duplication may underly the IPL phenotype (Figure 5A).

To determine if gene dosage is a general mechanism able to suppress SPB alleles, we were interested in determining if other mutants, like *cdc31-2*, would survive as haploids if an extra copy of the mutant gene was introduced at an ectopic site in the genome. We first tested the mutant allele with the phenotype most similar to *cdc31-2*: *kar1Δ17*, which contains a partial deletion in the Cdc31 binding domain (Vallen et al. 1994). Using a covered haploid strain, we integrated a single extra copy of *kar1Δ17* into the genome of the *kar1Δ17* mutant at a marker locus. A single extra copy of *kar1Δ17* suppressed diploidization at 23°C in a small fraction of cells; however, most cells were of higher ploidy (Figure 5B). Next, we examined other SPB mutant alleles that have a SPB duplication defect similar to *cdc31-2* (Vallen et al. 1994; Jaspersen, Giddings, and Winey 2002; Jaspersen et al. 2006; Chen et al. 2019; Winey et al. 1991; Kupke et al. 2011). An extra copy of *mps3-1* or *mps2-381* completely suppressed diploidization, similar to

359 *cdc31-2*, while *mps3-A540D* resulted in a partial rescue like *kar1*Δ*17* (Figure 5B).
360 Growth fitness improved in all the alleles with doubled gene copy number at all
361 temperatures. Although many mutants (*cdc31-2*, *mps3-1* and *mps2-381*) affecting
362 initiation of SPB duplication can be suppressed through the addition of an extra copy of
363 a mutant gene, increasing the dosage of other mutants only partially rescued IPL,
364 suggesting the nature of the mutation is important to dosage-based diploidization
365 suppression.
366
367 Examination of additional mutant alleles provided insights into the dosage-based
368 diploidization survival mechanism. Three *MPS3* alleles (*mps3-1*, *mps3-A540D* and
369 *mps3-W477A*) containing lesions in the C-terminal SUN domain that disrupt
370 nucleoskeleton and cytoskeleton (LINC) complex formation exhibit different degrees of
371 IPL suppression (Figure 5B). Interestingly, increasing the dosage of *mps3-W477A* poorly
372 suppressed its IPL phenotype. While this could be attributed to the allele, the fact that
373 the *mps3*Δ*2-150* mutant also shows a similar phenotype points to another contributing
374 factor. Unlike most *MPS3* alleles which are defective in initiation of SPB duplication,
375 *mps3-W477A* and *mps3*Δ*2-150* block SPB insertion (Figure 5A) (Friederichs et al. 2011;
376 Chen et al. 2019). Examination of two additional insertion mutants (*mps2-1* or *nbp1*Δ*AH*)
377 showed that extra copies of these genes also did not rescue IPL or restore growth when
378 added in extra copy (Figure 5A; data not shown). Collectively, these data support the
379 idea that spontaneous diploidization serves as a dosage suppressor for specific SPB
380 mutants that primarily affect initiation of SPB duplication.
381
382

Discussion

While lab strains of budding yeast are often maintained as stable haploid or diploid populations, polyploidy is common in natural yeast isolates (Ezov et al. 2006). The higher DNA state of triploid or diploid yeast allows for adaptation through the accumulation of mutations, some of which can be beneficial for fitness. However, higher ploidy is also associated with CIN, raising the question as to how cells maintain a stable ploidy.

Over the years, mutations in a number of pathways have been linked to spontaneous diploidization of haploid yeast strains, including: 1) mating type mutations, which restores the diploid state through mating-type switching (Lee et al. 2010); 2) cytokinetic mutants that fail in cell division to give rise to binucleate diploids (Rancati et al. 2008); and 3) spindle mutants that result in errors in chromosome segregation to produce mononuclear diploids (Sing et al. 2018; Luca and Winey 1998; Antoniacci et al. 2004; Chambers et al. 2012; Pinto and Winston 2000; Yu et al. 2011; Chan and Botstein 1993). Here, we investigated the IPL phenotype associated with certain mutations in the yeast SPB. Given SPB mutations are linked to chromosome segregation defects, an unresolved issue is why these alleles can be propagated as diploids under permissive conditions. While it is possible that tetraploids and octaploids do form, these higher ploidies are not detected for most alleles using flow cytometry. WGS of multiple SPB mutants also does not indicate disomes or other aneuploids are formed at least at the population level. For *cdc31-2* mutants, it was necessary to treat cells with a chemical mutagen and passage them through meiosis to create a disomic strain. This indicates that diploidization is the preferred ploidy of certain SPB mutants. Our goal was to understand the mechanism behind this ploidy regulation.

We describe how specific SPB mutations undergo dosage-based spontaneous diploidization. This phenotype is due, at least in part, to scaling of SPB architecture from haploid to diploid cells. Partial loss of function mutants that affect the first step of SPB duplication and whose gene products localize to SPB substructures that do no scale (luminal ring) or moderately scale (half-bridge) use diploidization to increase their copy number and to eliminate defects in SPB function at the permissive temperature. Thus, *cdc31-2*, *mps3-1* and *mps2-381* mutants are able to propagate as diploids. Importantly, extra copies of these genes do not overcome the growth defects and SPB phenotypes seen at higher temperatures, presumably because the mutant proteins are unstable at 37°C or the SPB duplication defect is not bypassed. Other SPB alleles such as *kar1Δ17*, *mps3-A540D*, *mps3-W477A* and *nbp1-AH* also show diploidization, but the IPL phenotype of haploids was not fully rescued by an additional copy of the mutant gene. While our ectopic rescue constructs may not express the gene at levels comparable to the endogenous locus, the fact that a disome did not suppress the IPL associated with *mps3-A540D* suggests a non-dosage dependent diploidization rescue pathway also exists.

In previous work, incompatible allometry within the spindle was linked with the CIN phenotype in *S. cerevisae* and other fungi (Jelenic et al. 2018; Hoyt, Stearns, and Botstein 1990). Although the surface area of the SPB increases to expand microtubule nucleation capacity, the length of the pre-anaphase spindle does not change in tetraploids compared to diploids even though tetraploid cells have twice the DNA content. As a result, the incidence of syntelic (monopolar) chromosome attachments is higher in tetraploids (Storchova et al. 2006). The loss of chromosomes from tetraploid *C. albicans* is so dramatic that it results in diploid or near diploid progeny (Bennett and Johnson 2003). Unlike the SPB core, we show here that the luminal ring does not

435 increase in size to a similar extent in diploids compared to haploids. This finding
436 strongly suggests that, similar to the NPC, this region of the SPB expands and contracts
437 via radial dilation. This mechanism of scaling could facilitate cell cycle changes in the
438 luminal ring size without the need to incorporate more protein. For example, in haploids
439 the SPB core size increases from 90 nm in G1 to 110 nm in mitosis (Byers and Goetsch
440 1974); radial expansion of the luminal ring would accommodate this increase without
441 incorporation of new protein. Similarly, as SPB size decreases back to 90 nm upon
442 anaphase exit, radial contraction of the SPB would allow the luminal ring to shrink by
443 increasing protein density.
444
445 In metazoans, centrosome function is regulated by factors involved in its duplication,
446 maturation and microtubule nucleation. Centrosomal defects are linked to errors in
447 chromosome segregation, in part due to the role of centrosomes in spindle organization.
448 However, centrosomes also contribute to the size of the mitotic spindle. Our work further
449 illustrates another possible role for centrosomes in driving genetic changes – the
450 acquisition of mutations in genes such as centrin, which is conserved throughout
451 eukaryotes, might promote stable genome amplification, including the genome
452 duplications seen throughout evolution in fungi and metazoans or during tumorigenesis
453 in humans.
454
455

Materials & Methods

Yeast strains and plasmids

All strains are derivatives of W303 (*ADE2 trp1-1 leu2-3,112 ura3-1 his3-11,15 can1-100 RAD5+*) and are listed in Table S2. Standard techniques were used for DNA and yeast manipulations, including C-terminal tagging with fluorescent proteins and gene deletion by PCR-based methods (Gardner and Jaspersen 2014). Single copy integrating plasmids containing SPB genes were made by PCR amplifying the open-reading frame, ~700 bp of promoter sequence and ~200 bp of the terminator from genomic DNA and assembling this DNA into pRG203MX using Gateway assembly (Gnugge, Liphardt, and Rudolf 2016). Mutations were introduced by site-directed mutagenesis of the wild-type gene using the QuikChange mutagenesis kit (Agilent). Sequencing was performed to confirm correct base pair substitutions or deletions were made.

Screen for cdc31-2 IPL suppressors

SLJ6749 (*MATα cdc31-2 CAN1::KANMX trp1Δ::NATMX cyh2 LYP1 ura3-1 his3-11,15 ade2-1 pURA3-CDC31*) was grown overnight at 30°C in SC-Ura plus casamino acids to an OD_{600} of ~2.0. Cells were harvested and individual aliquots were mutagenized with a dosage of EMS that resulted in ~50% lethality compared to an untreated control. Following mutagenesis, cells were plated to YPD at 23°C at which time individual colonies were cherry-picked into 96-well plates to allow for automated pinning using the Singer ROTOR (Singer Instruments). Next, loss of the *pURA3-CDC31* covering plasmid was selected by growing cells on 5-FOA for 3 d at 23°C. Mating to SLJ6750 (*MATa cdc31-2 can1Δ::STE2pr-HIS3MX CYH2 lyp1Δ::HYGMX ura3-1 trp1-1 his3-11,15 ade2-1*) was performed overnight on YPD; mated cells were selected by growth on YPD containing 200 µg/ml G418 and 300 µg/ml hygromycin for 3 d. Cells were transferred onto sporulation media for 3 weeks at 23°C. Meiotic progeny were selected by two

482 rounds of growth on SD-His-Lys-Arg containing 50 µg/ml canavanine, 50 µg/ml
483 thialysine and 10 µg/ml cycloheximide for 3 d at 23°C. Suppressors of *cdc31-2* IPL give
484 rise to colonies under these growth conditions.
485
486 From ~100,000 EMS mutagenized cells, 61 possible suppressors were identified. Flow
487 cytometric analysis of DNA content showed that 54 exhibited peaks at 1N and 2N, which
488 are typically observed in haploid yeast. Of these, we found using plasmid rescue, PCR
489 and sequencing that 43 contained mutations in the *URA3* gene on the covering plasmid
490 that allowed for growth on 5-FOA, thus these were false positives. The remaining 11
491 suppressors were analyzed by tetrad dissection to ensure that suppression segregates
492 2:2 through at least two crosses to SLJ6121 (*MATa cdc31-2 can1Δ::STE2pr-HIS3MX*
493 *TRP1 CYH2 ura3-1 his3-11,15 ade2-1 pURA3-CDC31*).
494
495 *Whole genome sequencing (WGS)*
496 Using 20 four-spored tetrads from a cross between an EMS-induced hit and SLJ6121,
497 we identified the two progeny from each tetrad that were diploid (control) and the two
498 progeny from each tetrad that were haploid (and therefore contained an ems hit). To
499 ensure equal representation of colonies, each was individually grown, normalized by
500 OD_{600}, then mixed to achieve equal number of all 40 cells in the control and ems hit
501 pools. Genomic libraries were prepared using the Illumina Mate Pair library kit and
502 prepared for paired-end sequencing on the Illumina MiSeq as previously described
503 (Birkeland et al. 2010). Downstream sequence analysis was performed (Birkeland et al.
504 2010). Reads were aligned to sacCer3 using bwa version 0.7.15-r1140 (Li and Durbin
505 2009) and single nucleotide polymorphisms (SNPs) and insertion/deletion
506 polymorphisms were identified using SAMtools version 1.5 (Li et al. 2009). SNP and
507 insertion/deletion polymorphisms were annotated using snpEff version 4.3 (Cingolani et

al. 2012). Coverage was calculated using BEDTools version 2.25.0 (Quinlan and Hall 2010). Results are listed in Table S1.

Flow cytometry and qPCR karyotyping

DNA content was analyzed by flow cytometry in sonicated cells that had been fixed with 70% ethanol for 1 h at room temperature, treated with RNAse (Roche, Basel, Switzerland) and Proteinase K (Roche) for 2 h to overnight at 37°C and stained with propidium iodide (Sigma-Aldrich, St. Louis) in the dark at 4°C overnight. Samples were analyzed on a MACSQuant FACS Analyzer (Miltenyi Biotec) and data was displayed using FlowJo software (Tree Star, Ashland, OR). qPCR karyotyping was performed using centromere proximal primers for each chromosome arm as previously described (Pavelka, Rancati, and Li 2010).

Growth assay

To analyze growth phenotypes, 5 OD_{600} of cells from each strain were serially diluted in 10-fold, and ~7 µl of each dilution was spotted on SD-Ura or SD plates containing 5-FOA (Sigma Aldrich). Plates were incubated at indicated temperatures for 2-4 days.

Image analysis

Live cell imaging was used to study spindle structure in cells containing GFP-Tub1 (microtubules) and Spc42-Cherry (SPBs) using a Perkin Elmer (Waltham, MA, USA) Ultraview spinning disk confocal microscope equipped with a Hamamatsu (Hamamatsu, Japan) EMCCD (C9100-13) optimized for speed, sensitivity and resolution. The microscope base was a Carl Zeiss (Jena, Germany) Axio-observer equipped with an αPlan-Apochromat 100x 1.46NA oil immersion objective and a multiband dichroic reflecting 488 and 561 nm laser lines. GFP images were acquired with 488 nm excitation

and 500-550 nm emission. mCherry images were acquired with 561 nm excitation and 580-650 nm emission. Data were acquired using the PerkinElmer Volocity software with a z spacing of 0.4 µm. Exposure time, laser power and camera gain were maintained at a constant level chosen to provide high signal-to-noise but avoid signal saturation for all samples. Images were processed using Image J (NIH, Bethesda, MD). A representative z slice image is shown. Cells were considered to be large-budded if the bud size was >30% the size of the mother cell.

Images for SPB intensity quantification in isogenic haploids and diploids were captured with a Nikon Spinning Disk controlled with NIS-Elements Viewer software equipped EMCCD camera and a PlanApo 100x 1.4 NA objective. Parameters, including laser power, exposure time, z-spacing and number of stacks, were set to identical value. Quantitation of levels of SPB proteins was performed with custom plugins (freely available at http://research.stowers.org/imagejplugins) written for ImageJ (NIH, Bethesda, MD). Prior to analysis, raw images were processed with background subtraction and summed to form a single plan image. Individual SPBs were identified using an ImageJ internal function “Find Maxima” and then chose “single points” as output. A circular ROI with a size of 7 pixel was drawn on each single point to cover individual SPB. Integrated intensity was then calculated on all ROIs.

Western blotting and quantification

Pelleted cells were washed in PBS and frozen in liquid nitrogen. Thawed pellets were resuspended in 1 ml lysis buffer (50 mM Tris, pH 7.5, 150 mM NaCl, 0.1%NP-40, 1 mM DTT, 10% glycerol and 1 mg/ml each pepstatin A, aprotinin and leupeptin) and ~100 µl of glass beads were added prior to bead beating for 1 min x 5 with 2 min on ice between beatings. Samples were spun at 5000 rpm for 2 min and the supernatant was transferred

560 to a new tube. Protein concentration was determined using a NanoDrop
561 Spectrophotometer (Thermo), and equivalent amounts of lysate were analyzed by SDS-
562 PAGE followed by western blotting. Whole cell extracts prepared by bead beating into
563 SDS sample buffer to determine expression levels of baits. The following primary
564 antibody dilutions were used: 1:1000 anti-Cdc31 (in the lab) and 1:5000 anti-Pgk1
565 (Invitrogen). Alkaline phosphatase-conjugated secondary antibodies were used at
566 1:10000 (Promega). Western blot band intensity was analyzed with ImageJ Gel
567 quantification tool.
568

569 **Acknowledgements**

570 We thank Giulia Rancati for strains and are grateful to Scott Hawley, Sarah Smith and
571 members of the Jaspersen Lab for helpful suggestions throughout the project and for
572 their comments on the manuscript. Original data underlying this manuscript can be
573 downloaded from the Stowers Original Data Repository at
574 http://www.stowers.org/research/publications/LIBPB-1533. Fastq files associated with
575 this project can be found at the National Center for Biotechnology Information
576 under BioProject ID PRJNA632749. Research reported in this publication was supported
577 by the Stowers Institute for Medical Research and the National Institute of General
578 Medical Sciences of the National Institutes of Health under award number
579 R01GM121443 (to SLJ). The authors declare no competing financial interests.
580

581 **Author contributions**

582 SLJ conceived the experiments, JC, ZX and AMC constructed strains, ZX performed the
583 screen, DMM analyzed genomic data and JC did the follow-up analysis. SM and WDB
584 did qPCR and automated flow cytometry analysis, and ZY acquired images and wrote

585 software for image quantitation. JC and SLJ prepared figures and wrote the paper with

586 input from all the authors.

587

588 **Abbreviations**

589 MTOC, microtubule-organizing center; SPB, spindle pole body; IPL, increase-in-ploidy;

590 CIN, chromosome instability; EMS, ethyl methanesulfonate; WGS, whole genome

591 sequencing; EM, electron microscopy; NE, nuclear envelope; NPC, nuclear pore

592 complex; FACS, Fluorescence-activated cell sorting; SEM, standard error of the mean;

593 5-FOA, 5-fluoro-orotic acid; SNP, single-nucleotide polymorphism

References

Adams, I. R., and J. V. Kilmartin. 1999. 'Localization of core spindle pole body (SPB) components during SPB duplication in Saccharomyces cerevisiae', *J Cell Biol*, 145: 809-23.

Amend, S. R., G. Torga, K. C. Lin, L. G. Kostecka, A. de Marzo, R. H. Austin, and K. J. Pienta. 2019. 'Polyploid giant cancer cells: Unrecognized actuators of tumorigenesis, metastasis, and resistance', *Prostate*, 79: 1489-97.

Anatskaya, O. V., and A. E. Vinogradov. 2007. 'Genome multiplication as adaptation to tissue survival: evidence from gene expression in mammalian heart and liver', *Genomics*, 89: 70-80.

Andalis, A. A., Z. Storchova, C. Styles, T. Galitski, D. Pellman, and G. R. Fink. 2004. 'Defects arising from whole-genome duplications in Saccharomyces cerevisiae', *Genetics*, 167: 1109-21.

Anderson, V. E., J. Prudden, S. Prochnik, T. H. Giddings, Jr., and K. G. Hardwick. 2007. 'Novel sfi1 alleles uncover additional functions for Sfi1p in bipolar spindle assembly and function', *Mol Biol Cell*, 18: 2047-56.

Antoniacci, L. M., M. A. Kenna, P. Uetz, S. Fields, and R. V. Skibbens. 2004. 'The spindle pole body assembly component mps3p/nep98p functions in sister chromatid cohesion', *J Biol Chem*, 279: 49542-50.

Bennett, R. J., and A. D. Johnson. 2003. 'Completion of a parasexual cycle in Candida albicans by induced chromosome loss in tetraploid strains', *EMBO J*, 22: 2505-15.

Birkeland, S. R., N. Jin, A. C. Ozdemir, R. H. Lyons, Jr., L. S. Weisman, and T. E. Wilson. 2010. 'Discovery of mutations in Saccharomyces cerevisiae by pooled linkage analysis and whole-genome sequencing', *Genetics*, 186: 1127-37.

Boeke, J. D., J. Trueheart, G. Natsoulis, and G. R. Fink. 1987. '5-Fluoroorotic acid as a selective agent in yeast molecular genetics', *Methods Enzymol*, 154: 164-75.

Bonney, M. E., H. Moriya, and A. Amon. 2015. 'Aneuploid proliferation defects in yeast are not driven by copy number changes of a few dosage-sensitive genes', *Genes Dev*, 29: 898-903.

Brachat, A., J. V. Kilmartin, A. Wach, and P. Philippsen. 1998. 'Saccharomyces cerevisiae cells with defective spindle pole body outer plaques accomplish nuclear migration via half-bridge-organized microtubules', *Mol Biol Cell*, 9: 977-91.

Byers, B., and L. Goetsch. 1974. 'Duplication of spindle plaques and integration of the yeast cell cycle', *Cold Spring Harb Symp Quant Biol*, 38: 123-31.

Cabral, G., T. Laos, J. Dumont, and A. Dammermann. 2019. 'Differential Requirements for Centrioles in Mitotic Centrosome Growth and Maintenance', *Dev Cell*, 50: 355-66 e6.

Cavanaugh, A. M., and S. L. Jaspersen. 2017. 'Big Lessons from Little Yeast: Budding and Fission Yeast Centrosome Structure, Duplication, and Function', *Annu Rev Genet*, 51: 361-83.

Chambers, A. L., G. Ormerod, S. C. Durley, T. L. Sing, G. W. Brown, N. A. Kent, and J. A. Downs. 2012. 'The INO80 chromatin remodeling complex prevents polyploidy and maintains normal chromatin structure at centromeres', *Genes Dev*, 26: 2590-603.

Chan, C. S., and D. Botstein. 1993. 'Isolation and characterization of chromosome-gain and increase-in-ploidy mutants in yeast', *Genetics*, 135: 677-91.

643 Chen, J., J. M. Gardner, Z. Yu, S. E. Smith, S. McKinney, B. D. Slaughter, J. R. Unruh,
644 and S. L. Jaspersen. 2019. 'Yeast centrosome components form a noncanonical
645 LINC complex at the nuclear envelope insertion site', *J Cell Biol*, 218: 1478-90.
646 Chen, J., C. J. Smoyer, B. D. Slaughter, J. R. Unruh, and S. L. Jaspersen. 2014. 'The
647 SUN protein Mps3 controls Ndc1 distribution and function on the nuclear
648 membrane', *J Cell Biol*, 204: 523-39.
649 Chen, L., and K. Madura. 2008. 'Centrin/Cdc31 is a novel regulator of protein
650 degradation', *Mol Cell Biol*, 28: 1829-40.
651 Chial, H. J., T. H. Giddings, Jr., E. A. Siewert, M. A. Hoyt, and M. Winey. 1999. 'Altered
652 dosage of the Saccharomyces cerevisiae spindle pole body duplication gene,
653 NDC1, leads to aneuploidy and polyploidy', *Proc Natl Acad Sci U S A*, 96: 10200-
654 5.
655 Cingolani, P., A. Platts, L. Wang le, M. Coon, T. Nguyen, L. Wang, S. J. Land, X. Lu, and
656 D. M. Ruden. 2012. 'A program for annotating and predicting the effects of single
657 nucleotide polymorphisms, SnpEff: SNPs in the genome of Drosophila
658 melanogaster strain w1118; iso-2; iso-3', *Fly (Austin)*, 6: 80-92.
659 Donaldson, A. D., and J. V. Kilmartin. 1996. 'Spc42p: a phosphorylated component of
660 the S. cerevisiae spindle pole body (SPD) with an essential function during SPB
661 duplication', *J Cell Biol*, 132: 887-901.
662 Elliott, S., M. Knop, G. Schlenstedt, and E. Schiebel. 1999. 'Spc29p is a component of
663 the Spc110p subcomplex and is essential for spindle pole body duplication', *Proc
664 Natl Acad Sci U S A*, 96: 6205-10.
665 Ezov, T. K., E. Boger-Nadjar, Z. Frenkel, I. Katsperovski, S. Kemeny, E. Nevo, A. Korol,
666 and Y. Kashi. 2006. 'Molecular-genetic biodiversity in a natural population of the
667 yeast Saccharomyces cerevisiae from "Evolution Canyon": microsatellite
668 polymorphism, ploidy and controversial sexual status', *Genetics*, 174: 1455-68.
669 Fischer, T., S. Rodriguez-Navarro, G. Pereira, A. Racz, E. Schiebel, and E. Hurt. 2004.
670 'Yeast centrin Cdc31 is linked to the nuclear mRNA export machinery', *Nat Cell
671 Biol*, 6: 840-8.
672 Friederichs, J. M., S. Ghosh, C. J. Smoyer, S. McCroskey, B. D. Miller, K. J. Weaver, K.
673 M. Delventhal, J. Unruh, B. D. Slaughter, and S. L. Jaspersen. 2011. 'The SUN
674 protein Mps3 is required for spindle pole body insertion into the nuclear
675 membrane and nuclear envelope homeostasis', *PLoS Genet*, 7: e1002365.
676 Fujiwara, T., M. Bandi, M. Nitta, E. V. Ivanova, R. T. Bronson, and D. Pellman. 2005.
677 'Cytokinesis failure generating tetraploids promotes tumorigenesis in p53-null
678 cells', *Nature*, 437: 1043-7.
679 Gardner, J. M., and S. L. Jaspersen. 2014. 'Manipulating the yeast genome: deletion,
680 mutation, and tagging by PCR', *Methods Mol Biol*, 1205: 45-78.
681 Geiser, J. R., H. A. Sundberg, B. H. Chang, E. G. Muller, and T. N. Davis. 1993. 'The
682 essential mitotic target of calmodulin is the 110-kilodalton component of the
683 spindle pole body in Saccharomyces cerevisiae', *Mol Cell Biol*, 13: 7913-24.
684 Geissler, S., G. Pereira, A. Spang, M. Knop, S. Soues, J. Kilmartin, and E. Schiebel.
685 1996. 'The spindle pole body component Spc98p interacts with the gamma-
686 tubulin-like Tub4p of Saccharomyces cerevisiae at the sites of microtubule
687 attachment', *EMBO J*, 15: 3899-911.
688 Gerstein, A. C., and S. P. Otto. 2009. 'Ploidy and the causes of genomic evolution', *J
689 Hered*, 100: 571-81.
690 Gianaroli, L., M. C. Magli, A. P. Ferraretti, and S. Munne. 1999. 'Preimplantation
691 diagnosis for aneuploidies in patients undergoing in vitro fertilization with a poor
692 prognosis: identification of the categories for which it should be proposed', *Fertil
693 Steril*, 72: 837-44.

694 Gnugge, R., T. Liphardt, and F. Rudolf. 2016. 'A shuttle vector series for precise genetic
695 engineering of Saccharomyces cerevisiae', *Yeast*, 33: 83-98.
696 Gordon, D. J., B. Resio, and D. Pellman. 2012. 'Causes and consequences of
697 aneuploidy in cancer', *Nat Rev Genet*, 13: 189-203.
698 Hara, Y., and A. Kimura. 2011. 'Cell-size-dependent control of organelle sizes during
699 development', *Results Probl Cell Differ*, 53: 93-108.
700 Harari, Y., Y. Ram, N. Rappoport, L. Hadany, and M. Kupiec. 2018. 'Spontaneous
701 Changes in Ploidy Are Common in Yeast', *Curr Biol*, 28: 825-35 e4.
702 Hartwell, L. H., R. K. Mortimer, J. Culotti, and M. Culotti. 1973. 'Genetic Control of the
703 Cell Division Cycle in Yeast: V. Genetic Analysis of cdc Mutants', *Genetics*, 74:
704 267-86.
705 Herskowitz, I. 1988. 'Life cycle of the budding yeast Saccharomyces cerevisiae',
706 *Microbiol Rev*, 52: 536-53.
707 Hoyt, M. A., T. Stearns, and D. Botstein. 1990. 'Chromosome instability mutants of
708 Saccharomyces cerevisiae that are defective in microtubule-mediated
709 processes', *Mol Cell Biol*, 10: 223-34.
710 Jaspersen, S. L., T. H. Giddings, Jr., and M. Winey. 2002. 'Mps3p is a novel component
711 of the yeast spindle pole body that interacts with the yeast centrin homologue
712 Cdc31p', *J Cell Biol*, 159: 945-56.
713 Jaspersen, S. L., A. E. Martin, G. Glazko, T. H. Giddings, Jr., G. Morgan, A. Mushegian,
714 and M. Winey. 2006. 'The Sad1-UNC-84 homology domain in Mps3 interacts with
715 Mps2 to connect the spindle pole body with the nuclear envelope', *J Cell Biol*,
716 174: 665-75.
717 Jelenic, I., A. Selmecki, L. Laan, and N. Pavin. 2018. 'Spindle Dynamics Model Explains
718 Chromosome Loss Rates in Yeast Polyploid Cells', *Front Genet*, 9: 296.
719 Joglekar, A. P., D. C. Bouck, J. N. Molk, K. S. Bloom, and E. D. Salmon. 2006.
720 'Molecular architecture of a kinetochore-microtubule attachment site', *Nat Cell
721 Biol*, 8: 581-5.
722 Kilmartin, J. V. 2003. 'Sfi1p has conserved centrin-binding sites and an essential function
723 in budding yeast spindle pole body duplication', *J Cell Biol*, 162: 1211-21.
724 Knop, M., G. Pereira, S. Geissler, K. Grein, and E. Schiebel. 1997. 'The spindle pole
725 body component Spc97p interacts with the gamma-tubulin of Saccharomyces
726 cerevisiae and functions in microtubule organization and spindle pole body
727 duplication', *EMBO J*, 16: 1550-64.
728 Kops, G. J., B. A. Weaver, and D. W. Cleveland. 2005. 'On the road to cancer:
729 aneuploidy and the mitotic checkpoint', *Nat Rev Cancer*, 5: 773-85.
730 Kupke, T., L. Di Cecco, H. M. Muller, A. Neuner, F. Adolf, F. Wieland, W. Nickel, and E.
731 Schiebel. 2011. 'Targeting of Nbp1 to the inner nuclear membrane is essential for
732 spindle pole body duplication', *EMBO J*, 30: 3337-52.
733 Lee, H. O., J. M. Davidson, and R. J. Duronio. 2009. 'Endoreplication: polyploidy with
734 purpose', *Genes Dev*, 23: 2461-77.
735 Lee, S. C., M. Ni, W. Li, C. Shertz, and J. Heitman. 2010. 'The evolution of sex: a
736 perspective from the fungal kingdom', *Microbiol Mol Biol Rev*, 74: 298-340.
737 Li, H., and R. Durbin. 2009. 'Fast and accurate short read alignment with Burrows-
738 Wheeler transform', *Bioinformatics*, 25: 1754-60.
739 Li, H., B. Handsaker, A. Wysoker, T. Fennell, J. Ruan, N. Homer, G. Marth, G. Abecasis,
740 R. Durbin, and Subgroup Genome Project Data Processing. 2009. 'The
741 Sequence Alignment/Map format and SAMTools', *Bioinformatics*, 25: 2078-9.
742 Liu, Z., S. Yue, X. Chen, T. Kubin, and T. Braun. 2010. 'Regulation of cardiomyocyte
743 polyploidy and multinucleation by CyclinG1', *Circ Res*, 106: 1498-506.

744 Luca, F. C., and M. Winey. 1998. 'MOB1, an essential yeast gene required for
745 completion of mitosis and maintenance of ploidy', *Mol Biol Cell*, 9: 29-46.
746 Marshall, W. F. 2011. 'Centrosome size: scaling without measuring', *Curr Biol*, 21: R594-
747 6.
748 Marteil, G., A. Guerrero, A. F. Vieira, B. P. de Almeida, P. Machado, S. Mendonca, M.
749 Mesquita, B. Villarreal, I. Fonseca, M. E. Francia, K. Dores, N. P. Martins, S. C.
750 Jana, E. M. Tranfield, N. L. Barbosa-Morais, J. Paredes, D. Pellman, S. A.
751 Godinho, and M. Bettencourt-Dias. 2018. 'Over-elongation of centrioles in cancer
752 promotes centriole amplification and chromosome missegregation', *Nat*
753 *Commun*, 9: 1258.
754 Mayer, V. W., and A. Aguilera. 1990. 'High levels of chromosome instability in polyploids
755 of Saccharomyces cerevisiae', *Mutat Res*, 231: 177-86.
756 Mittal, K., S. Donthamsetty, R. Kaur, C. Yang, M. V. Gupta, M. D. Reid, D. H. Choi, P. C.
757 G. Rida, and R. Aneja. 2017. 'Multinucleated polyploidy drives resistance to
758 Docetaxel chemotherapy in prostate cancer', *Br J Cancer*, 116: 1186-94.
759 Mulla, W., J. Zhu, and R. Li. 2014. 'Yeast: a simple model system to study complex
760 phenomena of aneuploidy', *FEMS Microbiol Rev*, 38: 201-12.
761 Myers, M. D., and G. S. Payne. 2017. 'Vps13 and Cdc31/centrin: Puzzling partners in
762 membrane traffic', *J Cell Biol*, 216: 299-301.
763 Nannas, N. J., E. T. O'Toole, M. Winey, and A. W. Murray. 2014. 'Chromosomal
764 attachments set length and microtubule number in the Saccharomyces
765 cerevisiae mitotic spindle', *Mol Biol Cell*, 25: 4034-48.
766 Oromendia, A. B., and A. Amon. 2014. 'Aneuploidy: implications for protein homeostasis
767 and disease', *Dis Model Mech*, 7: 15-20.
768 Orr-Weaver, T. L. 2015. 'When bigger is better: the role of polyploidy in organogenesis',
769 *Trends Genet*, 31: 307-15.
770 Otsuka, S., A. M. Steyer, M. Schorb, J. K. Heriche, M. J. Hossain, S. Sethi, M.
771 Kueblbeck, Y. Schwab, M. Beck, and J. Ellenberg. 2018. 'Postmitotic nuclear
772 pore assembly proceeds by radial dilation of small membrane openings', *Nat*
773 *Struct Mol Biol*, 25: 21-28.
774 Otto, S. P. 2007. 'The evolutionary consequences of polyploidy', *Cell*, 131: 452-62.
775 Pavelka, N., G. Rancati, and R. Li. 2010. 'Dr Jekyll and Mr Hyde: role of aneuploidy in
776 cellular adaptation and cancer', *Curr Opin Cell Biol*, 22: 809-15.
777 Pinto, I., and F. Winston. 2000. 'Histone H2A is required for normal centromere function
778 in Saccharomyces cerevisiae', *EMBO J*, 19: 1598-612.
779 Quinlan, A. R., and I. M. Hall. 2010. 'BEDTools: a flexible suite of utilities for comparing
780 genomic features', *Bioinformatics*, 26: 841-2.
781 Rancati, G., N. Pavelka, B. Fleharty, A. Noll, R. Trimble, K. Walton, A. Perera, K.
782 Staehling-Hampton, C. W. Seidel, and R. Li. 2008. 'Aneuploidy underlies rapid
783 adaptive evolution of yeast cells deprived of a conserved cytokinesis motor', *Cell*,
784 135: 879-93.
785 Ruthnick, D., and E. Schiebel. 2018. 'Duplication and Nuclear Envelope Insertion of the
786 Yeast Microtubule Organizing Centre, the Spindle Pole Body', *Cells*, 7.
787 Schild, D., H. N. Ananthaswamy, and R. K. Mortimer. 1981. 'An endomitotic effect of a
788 cell cycle mutation of Saccharomyces cerevisiae', *Genetics*, 97: 551-62.
789 Schramm, C., S. Elliott, A. Shevchenko, and E. Schiebel. 2000. 'The Bbp1p-Mps2p
790 complex connects the SPB to the nuclear envelope and is essential for SPB
791 duplication', *EMBO J*, 19: 421-33.
792 Selmecki, A., A. Forche, and J. Berman. 2006. 'Aneuploidy and isochromosome
793 formation in drug-resistant Candida albicans', *Science*, 313: 367-70.

794 Selmecki, A. M., Y. E. Maruvka, P. A. Richmond, M. Guillet, N. Shoresh, A. L. Sorenson,
795 S. De, R. Kishony, F. Michor, R. Dowell, and D. Pellman. 2015. 'Polyploidy can
796 drive rapid adaptation in yeast', *Nature*, 519: 349-52.
797 Shahin, V., L. Albermann, H. Schillers, L. Kastrup, C. Schafer, Y. Ludwig, C. Stock, and
798 H. Oberleithner. 2005. 'Steroids dilate nuclear pores imaged with atomic force
799 microscopy', *J Cell Physiol*, 202: 591-601.
800 Sheltzer, J. M., and A. Amon. 2011. 'The aneuploidy paradox: costs and benefits of an
801 incorrect karyotype', *Trends Genet*, 27: 446-53.
802 Shimizu, Y., T. Akashi, A. Okuda, A. Kikuchi, and K. Fukui. 2000. 'NBP1 (Nap1 binding
803 protein 1), an essential gene for G2/M transition of Saccharomyces cerevisiae,
804 encodes a protein of distinct sub-nuclear localization', *Gene*, 246: 395-404.
805 Sing, T. L., M. P. Hung, S. Ohnuki, G. Suzuki, B. J. San Luis, M. McClain, J. R. Unruh,
806 Z. Yu, J. Ou, J. Marshall-Sheppard, W. K. Huh, M. Costanzo, C. Boone, Y. Ohya,
807 S. L. Jaspersen, and G. W. Brown. 2018. 'The budding yeast RSC complex
808 maintains ploidy by promoting spindle pole body insertion', *J Cell Biol*, 217: 2445-
809 62.
810 Soltis, P. S., D. B. Marchant, Y. Van de Peer, and D. E. Soltis. 2015. 'Polyploidy and
811 genome evolution in plants', *Curr Opin Genet Dev*, 35: 119-25.
812 Spang, A., S. Geissler, K. Grein, and E. Schiebel. 1996. 'gamma-Tubulin-like Tub4p of
813 Saccharomyces cerevisiae is associated with the spindle pole body
814 substructures that organize microtubules and is required for mitotic spindle
815 formation', *J Cell Biol*, 134: 429-41.
816 Storchova, Z. 2014. 'Ploidy changes and genome stability in yeast', *Yeast*, 31: 421-30.
817 Storchova, Z., A. Breneman, J. Cande, J. Dunn, K. Burbank, E. O'Toole, and D.
818 Pellman. 2006. 'Genome-wide genetic analysis of polyploidy in yeast', *Nature*,
819 443: 541-7.
820 Storchova, Z., and D. Pellman. 2004. 'From polyploidy to aneuploidy, genome instability
821 and cancer', *Nat Rev Mol Cell Biol*, 5: 45-54.
822 Sundberg, H. A., L. Goetsch, B. Byers, and T. N. Davis. 1996. 'Role of calmodulin and
823 Spc110p interaction in the proper assembly of spindle pole body compenents', *J*
824 *Cell Biol*, 133: 111-24.
825 Thomas, J. H., and D. Botstein. 1986. 'A gene required for the separation of
826 chromosomes on the spindle apparatus in yeast', *Cell*, 44: 65-76.
827 Torres, E. M., N. Dephoure, A. Panneerselvam, C. M. Tucker, C. A. Whittaker, S. P.
828 Gygi, M. J. Dunham, and A. Amon. 2010. 'Identification of aneuploidy-tolerating
829 mutations', *Cell*, 143: 71-83.
830 Torres, E. M., T. Sokolsky, C. M. Tucker, L. Y. Chan, M. Boselli, M. J. Dunham, and A.
831 Amon. 2007. 'Effects of aneuploidy on cellular physiology and cell division in
832 haploid yeast', *Science*, 317: 916-24.
833 Vallen, E. A., W. Ho, M. Winey, and M. D. Rose. 1994. 'Genetic interactions between
834 CDC31 and KAR1, two genes required for duplication of the microtubule
835 organizing center in Saccharomyces cerevisiae', *Genetics*, 137: 407-22.
836 Varberg, J. M., and S. L. Jaspersen. 2018. 'To Make a Long Spindle Short: Nuclear
837 Envelope Breakdown during Meiosis', *Cell Rep*, 23: 931-32.
838 Vitre, B. D., and D. W. Cleveland. 2012. 'Centrosomes, chromosome instability (CIN)
839 and aneuploidy', *Curr Opin Cell Biol*, 24: 809-15.
840 Wang, T. L., C. Maierhofer, M. R. Speicher, C. Lengauer, B. Vogelstein, K. W. Kinzler,
841 and V. E. Velculescu. 2002. 'Digital karyotyping', *Proc Natl Acad Sci U S A*, 99:
842 16156-61.

Winey, M., L. Goetsch, P. Baum, and B. Byers. 1991. 'MPS1 and MPS2: novel yeast genes defining distinct steps of spindle pole body duplication', *J Cell Biol*, 114: 745-54.

Winey, M., M. A. Hoyt, C. Chan, L. Goetsch, D. Botstein, and B. Byers. 1993. 'NDC1: a nuclear periphery component required for yeast spindle pole body duplication', *J Cell Biol*, 122: 743-51.

Yoder, T. J., C. G. Pearson, K. Bloom, and T. N. Davis. 2003. 'The Saccharomyces cerevisiae spindle pole body is a dynamic structure', *Mol Biol Cell*, 14: 3494-505.

Yu, Y., M. Srinivasan, S. Nakanishi, J. Leatherwood, A. Shilatifard, and R. Sternglanz. 2011. 'A conserved patch near the C terminus of histone H4 is required for genome stability in budding yeast', *Mol Cell Biol*, 31: 2311-25.

Figures

Figure 1. Spontaneous diploidization of SPB mutants such as *cdc31-2* at the permissive temperature. (A) Wild-type (SLJ7819) and *cdc31-2* mutant (SLJ10777) cells containing GFP-Tub1 (white) and Spc42-mCherry (magenta) were generated with a *pURA3-CDC31* plasmid. After growth on 5-FOA at 23°C to select for loss of the plasmid, the *cdc31-2* mutant spontaneously diploidize despite the formation of bipolar spindles. A representative image from each is shown (bar = 2 μm), and the percentage of large budded cells for with bipolar, monopolar or multipolar/broken spindles was quantitated (n>150). DNA content was assayed by flow cytometry. The biphasic peaks in wild-type cells represent cells with G1 (1N) and G2/M (2N) DNA content. At 23°C, *cdc31-2* mutants have diploid DNA content (2N and 4N). (B) Schematic of pathway to diploidization in *cdc31-2*. Due to a defect in chromosome segregation, haploid (1N) cells undergo an aberrant cell division to produce a diploid (2N) and aploid (0N) cell. The diploid cell does not have the same defect as haploids, resulting in successfully propagation. Because of this, we suspect that a suppressor mutation is acquired.

Figure 2. Screen for suppressors of *cdc31-2* diploidization. (A) Suppressors of the *cdc31-2* increase-in-ploidy were isolated following mutagenesis of SLJ6749 (*MATα cdc31-2 CAN1::KANMX trp1Δ::KANMX cyh2 LYP1 ura3-1 his3-11,15 ade2-1 pURA3-CDC31*) to ~50% viability using EMS. Loss of the *pURA3-CDC31* covering plasmid was selected using 5-FOA; strains without a suppressor will spontaneously diploidize as shown in Figure 1 while those with a suppressor will remain haploid. (B) Haploid (1N) or diploid (2N) strains can be mated to a haploid to form diploid (2N) or triploid (3N) cells. The viability of meiotic products is high from diploids (88.2%, n=40 tetrads) compared to triploids (6.2%, 40 tetrads). Using this property, suppressors of diploidization were selected by mating to SLJ6750 (*MATa CDC31 can1Δ::STE2pr-HIS3MX CYH2*

882 *lyp1Δ::HYGMX ura3-1 trp1-1 his3-11,15 ade2-1*) on YPD + G418 + Hyg. Following
883 sporulation, haploid selection was carried out using SD-His-Lys-
884 Arg+canavanine+thialysine+cycloheximide. (C) From ~100,000 EMS mutagenized cells,
885 61 possible suppressors were identified, and 54 were confirmed to be haploids in a
886 secondary screen of the original mutagenized colonies by flow cytometric analysis of
887 DNA content. Of these, 43 appeared to have mutations in the covering plasmid that
888 allowed for growth. The remaining 11 suppressors were analyzed by tetrad dissection to
889 ensure that suppression segregates 2:2 through at least two crosses to SLJ6121 (*MATa*
890 *cdc31-2 can1Δ::STE2pr-HIS3MX TRP1 CYH2 ura3-1 his3-11,15 ade2-1 pURA3-*
891 *CDC31*). An example of flow cytometry data from one hit is shown. (D) Coverage ratio
892 of all 16 yeast chromosomes in the haploid suppressors (*ems7*, *ems9*, or *ems11*)
893 relative to the diploid control (*EMS7*, *EMS9*, *EMS11*). Other single nucleotide
894 polymorphisms and insertions/deletion polymorphisms identified in the haploid
895 suppressors are listed in Table S1. (E) Quantitative PCR was performed on all 11
896 suppressors to determine the mean copy number of all 16 chromosomes relative to a
897 wild-type, with chromosome XV plotted in red. Error bars, standard deviation from the
898 mean.
899
900 **Figure 3. An extra copy of the *cdc31-2* gene is necessary and sufficient to**
901 **suppress IPL.** (A) To test if an extra copy of *cdc31-2* is necessary to suppress IPL, one
902 copy of the *cdc31-2* locus was deleted in cells a chromosome XV disome homozygous
903 for *cdc31-2*, was illustrated in the schematic. (B-C) The DNA content (B) and growth (C)
904 of wild-type (SLJ7249), *cdc31-2* (SLJ809), the chromosome XV *cdc31-2* disome
905 (SLJ7106, *cdc31-2 2xChXV(cdc31-2)*) and the deletion ((SLJ7111, *cdc31-2*
906 *ChXV(cdc31-2Δ::KANMX)*) that contain *pURA3-CDC31* were compared after growth in
907 SD-Ura or 5-FOA at the indicated temperatures. (D) To test if an extra copy of *cdc31-2* is

908 sufficient to suppress IPL, one additional copy of *cdc31-2* was inserted into the *HIS3*
909 locus on chromosome XV. (E-F) The DNA content (E) and growth (F) of wild-type
910 (SLJ7249), *cdc31-2* (SLJ809) and *cdc31-2* with an empty vector, wild-type, *CDC31* or
911 *cdc31-2* at *HIS3* (SLJ13092, SLJ13093 or SLJ13094) were analyzed after growth in SD-
912 Ura or 5-FOA at the indicated temperatures.
913
914 **Figure 4. Scaling of SPB components with ploidy.** (A) Schematic of the SPB showing
915 the location of the core, luminal ring and half-bridge. (B) Side and top-down views of the
916 SPB from haploids and diploids along with dimensions reported from EM measurements.
917 Assuming the SPB is round and the bridge elliptical and limited to a single protein layer,
918 theoretical scaling factors can be calculated. Based on dimensions calculated from EM
919 measurements, which are shown, a single layer of protein in the SPB core would be 2.11
920 times larger in diploids. The half-bridge is thought to be a monolayer of constant length
921 in both haploids and diploids, however, its width may scale. Two potential models for
922 scaling of the luminal ring are depicted: a continuous scaling, where components
923 increase proportionally to the circumference of the SPB core (1.45-fold); or radial
924 dilation, where the amount of components do not increase. (C) Levels of fluorophore
925 tagged protein derivatives expressed from endogenous loci in haploids or homozygous
926 diploids were determined by quantitative imaging. For each protein, levels in haploid
927 cells were normalized to 1. Errors, SEM with N>300 for each sample. (D) To determine
928 levels of Cdc31, western blotting was performed using anti-Cdc31 antibody. Pgk1 served
929 as a loading control.
930
931 **Figure 5. Dosage and IPL in other SPB mutants.** (A) Schematic of SPB duplication
932 pathway from an unduplicated SPB to duplicated side-by-side SPBs. Mutants defective
933 in initiation, maturation and insertion of the new SPB have been isolated; shown are

934 alleles required at each step that also exhibit IPL at 23°C (see Table 1). (B) To test if an
935 extra copy of these mutant genes is sufficient to suppress IPL, one additional copy was
936 inserted into the *HIS3* locus on chromosome XV as in Figure 3D-F. The growth and DNA
937 content of wild-type, mutant and mutant with an empty vector, wild-type gene or mutant
938 gene at *HIS3* were analyzed after growth in SD-Ura or 5-FOA at the indicated
939 temperatures.
940

Tables

Table 1. Ploidy level and function of *spb ts* alleles at 23°C in W303

SPB *ts* alleles	Ploidy at 23°C	Localization at SPB*	References
cdc31-2	2N/4N	half-bridge	(Schild, Ananthaswamy, and Mortimer 1981)
CDC31-16	1N/2N	half-bridge	(Vallen et al. 1994)
kar1Δ17	2N/4N	half-bridge	(Vallen et al. 1994)
sfi1-3	1N/2N	half-bridge	(Anderson et al. 2007)
sfi1-7	1N/2N	half-bridge	(Anderson et al. 2007)
mps3-1	2N/4N	half-bridge & luminal ring	(Jaspersen, Giddings, and Winey 2002)
mps3-W477A	2N/4N	half-bridge & luminal ring	(Jaspersen et al. 2006)
mps3-W487A	1N/2N	half-bridge & luminal ring	(Jaspersen et al. 2006)
msp3-Y502H	1N/2N	half-bridge & luminal ring	(Jaspersen et al. 2006)
mps3-A540D	2N/4N	half-bridge & luminal ring	(Jaspersen et al. 2006)
mps3-F592S	1N/2N	half-bridge & luminal ring	(Jaspersen et al. 2006)
mps3Δ2-150	2N/4N	half-bridge & luminal ring	(Chen et al. 2019)
mps2-1	2N/4N	luminal ring	(Winey et al. 1991)
mps2-381	2N/4N	luminal ring	(Jaspersen et al. 2006)
ndc1-A290E	1N/2N	luminal ring	(Chen et al. 2014)
ndc1-39	1N/2N	luminal ring	(Chen et al. 2014)
ndc1-1	1N/2N	luminal ring	(Thomas and Botstein 1986)
bbp1-1	1N/2N	luminal ring	(Schramm et al. 2000)
nbp1-1	1N/2N	luminal ring	(Shimizu et al. 2000)
nbp1-ΔAH	2N/4N	luminal ring	(Kupke et al. 2011)
cnm67Δ	1N/2N	core	(Brachat et al. 1998)
spc42-11	1N/2N	core	(Donaldson and Kilmartin 1996)
spc29-3	1N/2N	core	(Elliott et al. 1999)
cmd1-1	1N/2N	core	(Geiser et al. 1993)
spc110-220	1N/2N	core	(Sundberg et al. 1996)
spc97-14	1N/2N	core	(Knop et al. 1997)
spc97-20	1N/2N	core	(Knop et al. 1997)
spc98-2	1N/2N	core	(Geissler et al. 1996)
tub4-1	1N/2N	core	(Spang et al. 1996)

* inner, central and outer plaque localization is denoted the core

944 **Supplementary Material**

945 Table S1. Single nucleotide and insertion/deletion polymorphisms annotated with SnpEff

946 for three *cdc31* suppressors

947 Table S2. Yeast strains

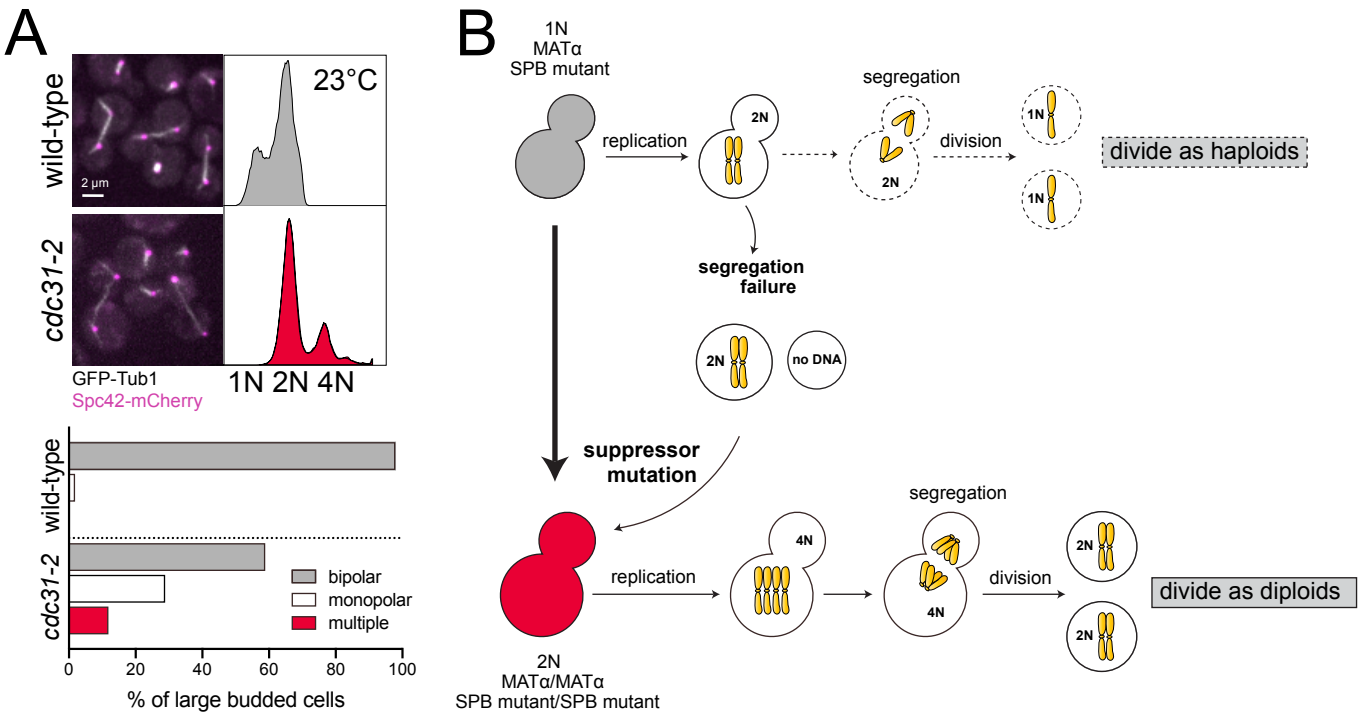

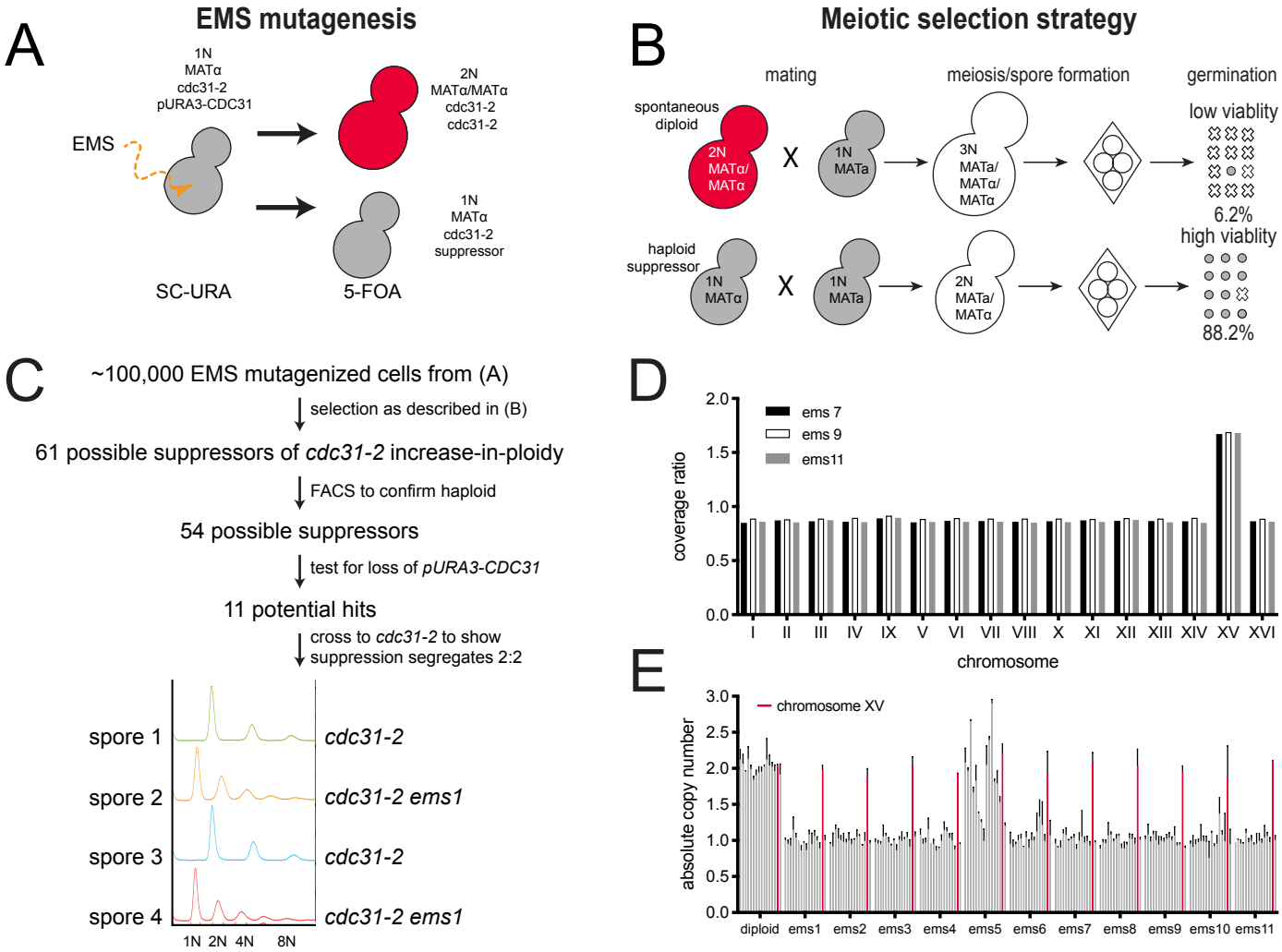

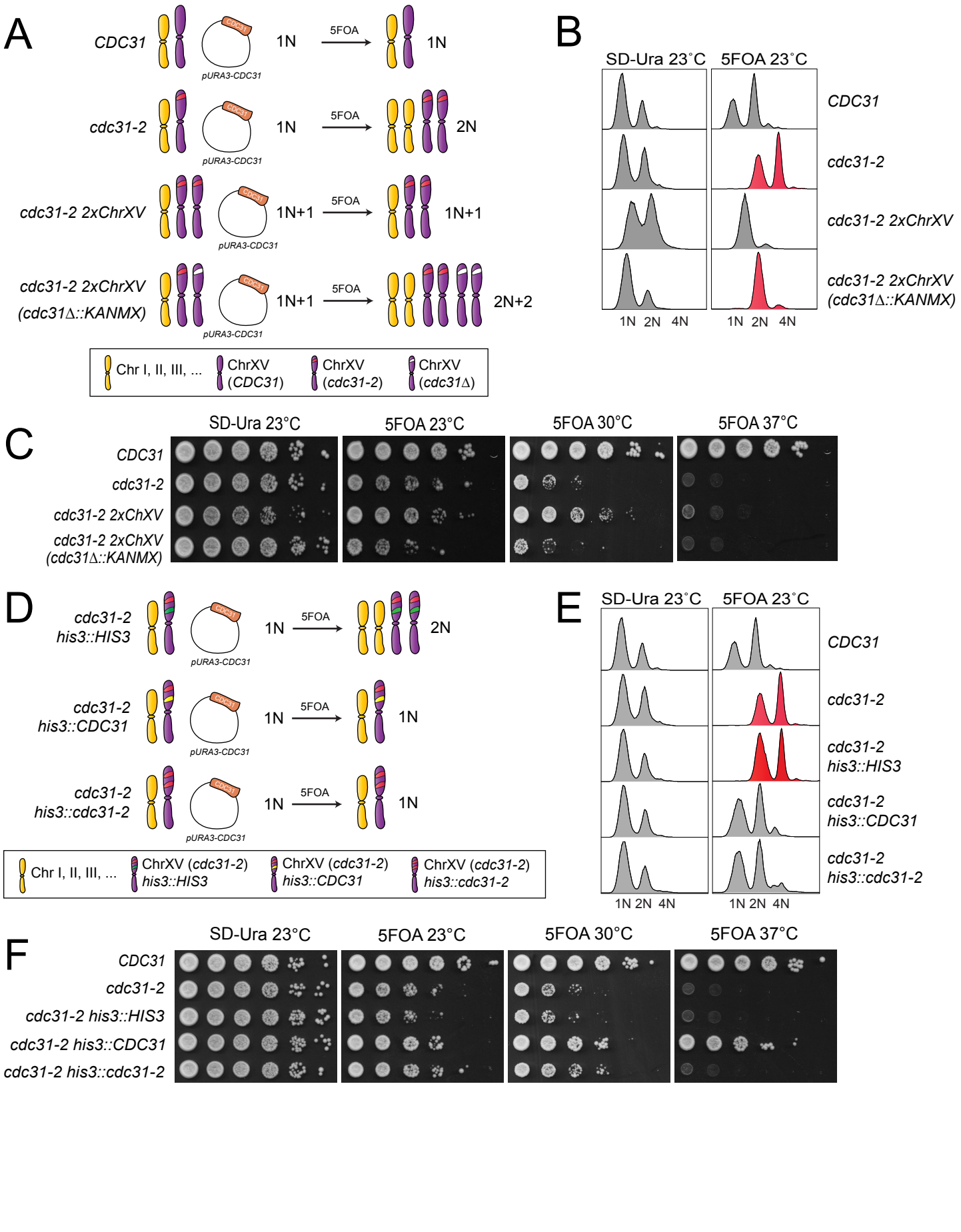

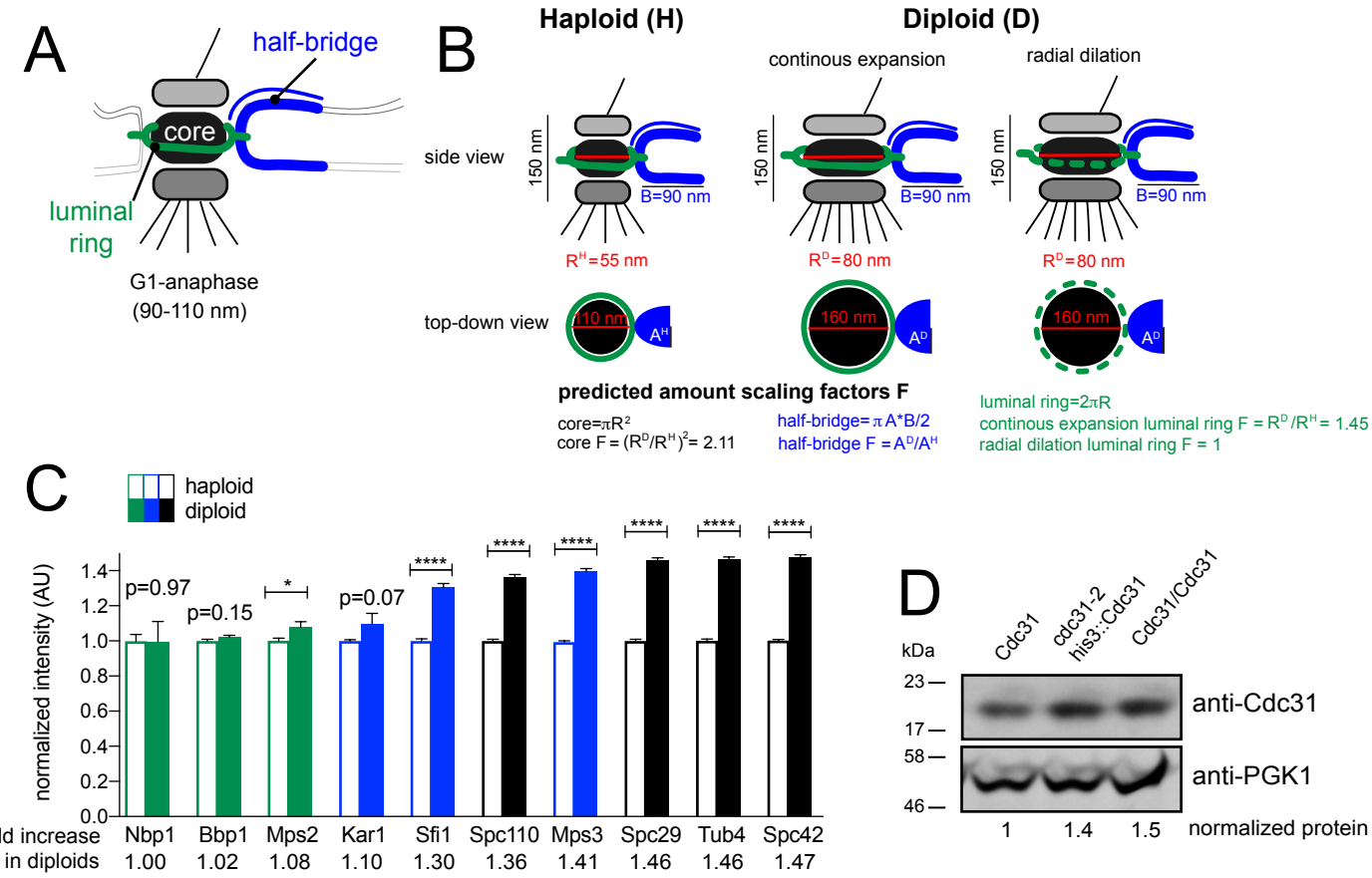

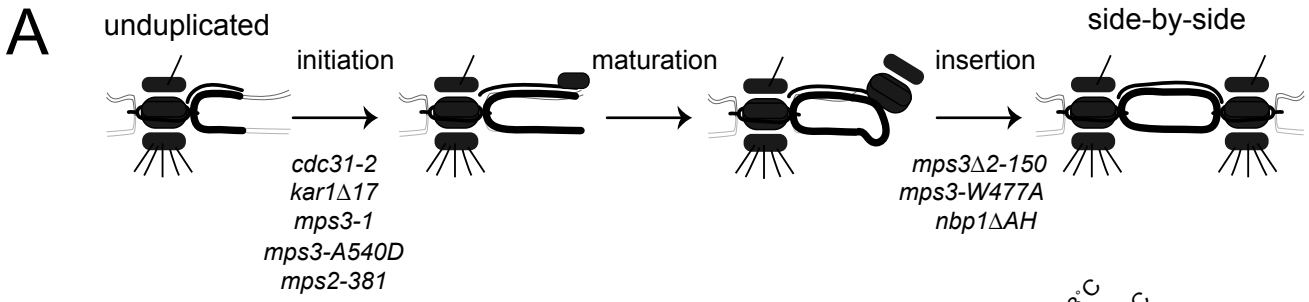

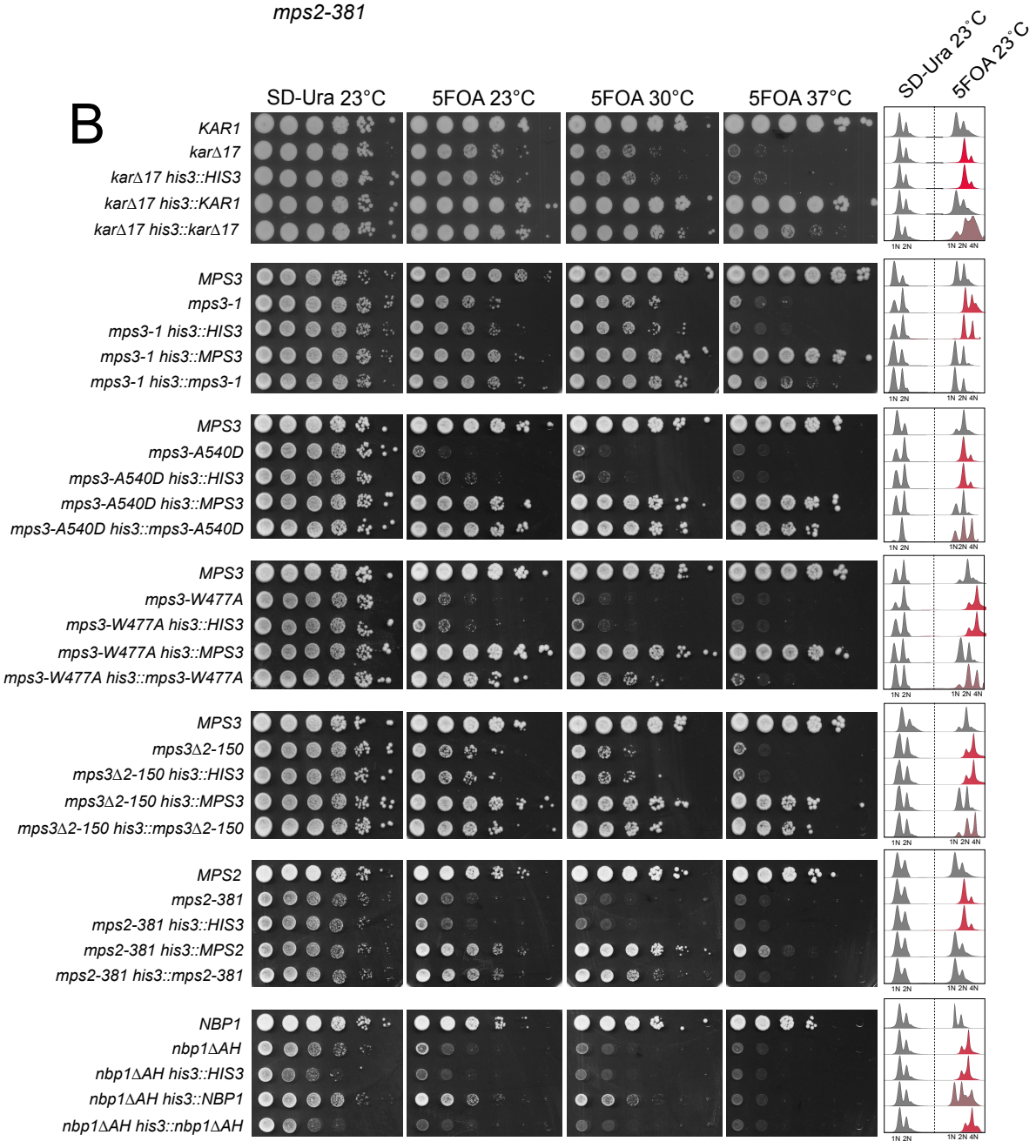

Table S1. Location of *cdc31-2* IPL suppressors*.

Chromosome	Position	Reference	Change	VCF Score	Location	Gene	Protein Change	Type
cdc31-2 ems7								
XVI	769362	T	C	222	intergenic	na	na	na
cdc31-2 ems9								
III	307421	G	A	225	intergenic	na	na	na
III	307422	C	A	225	intergenic	na	na	na
IX	438797	C	T	222	intergenic	na	na	na
V	6586	A	G	222	intergenic	na	na	na
V	6594	T	C	221	intergenic	na	na	na
V	6600	A	G	221	intergenic	na	na	na
VI	92485	C	T	222	genic	*BUD27*	V500V	synonymous
X	354706	T	C	219	intergenic	na	na	na
XIII	587695	T	C	205	intergenic	na	na	na
cdc31-2 ems11								
XVI	769362	T	C	222	intergenic	na	na	na
XVI	769434	T	G	222	intergenic	na	na	na

* shown are variants detected in the genome of the mutant compared to control.

Table S2. Yeast strains

Strain	Relevant genotype[a]	Figure
SLJ001	*MATa bar1- ura3-1 trp1-1 leu2-3,115 his3-11,15 ade2-1 can1-100*	1A, 5C
SLJ1070	*MATa/α bar1- ura3-1 trp1-1 leu2-3,115 his3-11,15 ade2-1 can1-100*	4D
SLJ0809	*MATa cdc31-2 pURA3-CDC31*	1A, 3A, 3C, 4D
SLJ7819	*MATα SPC42-mCherry-HYGMX GFP-Tub1-NATMX*	1A-B
SLJ10777	*MATa cdc31-2 SPC42-mCherry-HYGMX GFP-Tub1-NATMX pURA3-CDC31*	1A-B
SLJ6750	*MATa cdc31-2 can1Δ::STE2pr-HIS3MX lyp1Δ::HYGMX CYH2*	2C-E
SLJ6749	*MATα cdc31-2 CAN1::KANMX trp1Δ::NATMX cyh2 LYP1 pURA3-CDC31*	2C-E
SLJ6735	*MATα trp1Δ::NATMX CAN1-KANMX cyh2 ems1*	2C-E
SLJ6736	*MATα trp1Δ::NATMX CAN1-KANMX cyh2 ems2*	2C-E
SLJ6737	*MATα trp1Δ::NATMX CAN1-KANMX cyh2 ems3*	2C-E
SLJ6738	*MATα trp1Δ::NATMX CAN1-KANMX cyh2 ems4*	2C-E
SLJ6739	*MATα trp1Δ::NATMX CAN1-KANMX cyh2 ems5*	2C-E
SLJ6740	*MATα trp1Δ::NATMX CAN1-KANMX cyh2 ems6*	2C-E
SLJ6741	*MATα trp1Δ::NATMX CAN1-KANMX cyh2 ems7*	2C-E
SLJ6742	*MATα trp1Δ::NATMX CAN1-KANMX cyh2 ems8*	2C-E
SLJ6743	*MATα trp1Δ::NATMX CAN1-KANMX cyh2 ems9*	2C-E
SLJ6744	*MATα trp1Δ::NATMX CAN1-KANMX cyh2 ems10*	2C-E
SLJ6745	*MATα trp1Δ::NATMX CAN1-KANMX cyh2 ems11*	2C-E
SLJ6746	*MATα trp1Δ::NATMX CAN1-KANMX cyh2 ems12*	2C-E
SLJ6121	*MATa cdc31-2 can1Δ::STE2pr-HIS3MX TRP1 CYH2 pURA3-CDC31*	2C-E
SLJ7106	*MATα cdc31-2 CAN1-KANMX extra ChXV*	3A-C
SLJ7111	*MATα/α cdc31-2/cdc31-2Δ::NATMX CAN1-KANMX extra ChXV*	3A-C
SLJ7249	*MATα pURA3-CDC31*	3A-C, D-F
SLJ13092	*MATa cdc31-2 his3-11,15::pRG203MX pURA3-CDC31*	3D-F
SLJ13093	*MATa cdc31-2 his3-11,15::pRG203MX-CDC31 pURA3-CDC31*	3D-F, 4D
SLJ13094	*MATa cdc31-2 his3-11,15::pRG203MX-cdc31-2 pURA3-CDC31*	3D-F
SLJ6991	*MATα NBP1-mTurquoise2-URA3MX*	4C
SLJ7100	*MATa/a NBP1-mTurquoise-URA3MX/NBP1-mTurquoise2-URA3MX*	4C
SLJ6986	*MATa BBP1-YFP-HIS3MX*	4C
SLJ11154	*MATa/α BBP1-YFP-HIS3MX/BBP1-YFP-HIS3MX*	4C
SLJ8657	*MATa MPS2-YFP-HIS3MX*	4C
SLJ11355	*MATa/α MPS2-YFP-HIS3MX/MPS2-YFP-HIS3MX*	4C
SLJ8539	*MATa MPS3-YFP-HIS3MX*	4C
SLJ11325	*MATa/α MPS3-YFP-HIS3MX/MPS3-YFP-HIS3MX*	4C
SLJ1091	*MATa YFP-KAR1*	4C
SLJ1119	*MATa/α YFP-KAR1/YFP-KAR1*	4C
SLJ1000	*MATa SPC110-YFP-HIS3MX*	4C
SLJ11152	*MATa/α SPC110-YFP-HIS3MX/SPC110-YFP-HIS3MX*	4C

SLJ1004	*MATa SPC29-YFP-HIS3MX*	4C
SLJ11150	*MATa/α SPC29-YFP-HIS3MX/SPC29-YFP-HIS3MX*	4C
SLJ9105	*MATa Tub4-YFP-HIS3MX*	4C
SLJ11153	*MATa/α Tub4-YFP-HIS3MX/Tub4-YFP-HIS3MX*	4C
SLJ8537	*MATa SPC42-YFP-HIS3MX*	4C
SLJ11149	*MATa/α SPC42-YFP-HIS3MX/SPC42-YFP-HIS3MX*	4C
SLJ7538	*MATa pURA3-KAR1*	5B
SLJ0843	*MATa kar1Δ17 pURA3-KAR1*	5B
SLJ13222	*MATa kar1Δ17 his3-11,15::pRG203MX pURA3-KAR1*	5B
SLJ13223	*MATa kar1Δ17 his3-11,15::pRG203MX-KAR1 pURA3-KAR1*	5B
SLJ13224	*MATa kar1Δ17 his3-11,15::pRG203MX-kar1Δ17 pURA3-KAR1*	5B
SLJ7250	*MATα pURA-MPS3*	5B
SLJ6026	*MATa mps3-1 pURA-MPS3*	5B
SLJ13105	*MATa mps3-1 his3-11,15::pRG203MX pURA3-MPS3*	5B
SLJ13106	*MATa mps3-1 his3-11,15::pRG203MX-MPS3 pURA3-MPS3*	5B
SLJ13107	*MATa mps3-1 his3-11,15::pRG203MX-mps3-1 pURA3-MPS3*	5B
SLJ2123	*MATa mps3Δ::NATMX trp1::mps3-A540D-12xMYC-TRP1 pURA3-MPS3*	5B
SLJ13149	*MATa mps3Δ::NATMX trp1::mps3-A540D-12xMYC-TRP1 his3-11,15::pRG203MX pURA3-MPS3*	5B
SLJ13150	*MATa mps3Δ::NATMX trp1::mps3-A540D-12xMYC-TRP1 his3-11,15::pRG203MX-MPS3 pURA3-MPS3*	5B
SLJ13151	*MATa mps3Δ::NATMX trp1::mps3-A540D-12xMYC-TRP1 his3-11,15::pRG203MX-mps3-A540D pURA3-MPS3*	5B
SLJ2117	*MATa mps3Δ::NATMX trp1::mps3-W477A-12xMYC-TRP1 pURA3-MPS3*	5B
SLJ13140	*MATa mps3Δ::NATMX trp1::mps3-W477A-12xMYC-TRP1 his3-11,15::pRG203MX pURA3-MPS3*	5B
SLJ13141	*MATa mps3Δ::NATMX trp1::mps3-W477A-12xMYC-TRP1 his3-11,15::pRG203MX-MPS3 pURA3-MPS3*	5B
SLJ13142	*MATa mps3Δ::NATMX trp1::mps3-W477A-12xMYC-TRP1 his3-11,15::pRG203MX-mps3-W477A pURA3-MPS3*	5B
SLJ13098	*MATa mps3Δ::NATMX leu2::mps3Δ2-150-LEU2 pURA3-MPS3*	5B
SLJ13192	*MATa mps3Δ::NATMX leu2::mps3Δ2-150-LEU2 his3-11,15::pRG203MX pURA3-MPS3*	5B
SLJ13193	*MATa mps3Δ::NATMX leu2::mps3Δ2-150-LEU2 his3-11,15::pRG203MX-MPS3 pURA3-MPS3*	5B
SLJ13194	*MATa mps3Δ::NATMX leu2::mps3Δ2-150-LEU2 his3-11,15::pRG203MX-mps3Δ2-150 pURA3-MPS3*	5B
SLJ7252	*MATα pURA-MPS2*	5B
SLJ12605	*MATa mps2Δ::NATMX leu2::mps2-381-KANMX pURA-MPS2*	5B
SLJ13146	*MATa mps2Δ::NATMX leu2::mps2-381-KANMX his3-11,15::pRG203MX pURA-MPS2*	5B
SLJ13147	*MATa mps2Δ::NATMX leu2::mps2-381-KANMX his3-11,15::pRG203MX-MPS2 pURA-MPS2*	5B
SLJ13148	*MATa mps2Δ::NATMX leu2::mps2-381-KANMX his3-11,15::pRG203MX-mps2-381 pURA-MPS2*	5B
SLJ13103	*MATa nbp1Δ::NATMX trp1::NBP1-TRP1 pURA3-ADE3-NBP1*	5B

SLJ13104	*MATa nbp1Δ::NATMX trp1::nbp1ΔAH-TRP1 pURA3-ADE3-NBP1*	5B
SLJ13131	*MATa nbp1Δ::NATMX trp1::nbp1ΔAH-TRP1 his3-11,15::pRG203MX pURA3-ADE3-NBP1*	5B
SLJ13132	*MATa nbp1Δ::NATMX trp1::nbp1ΔAH-TRP1 his3-11,15::pRG203MX-NBP1 pURA3-ADE3-NBP1*	5B
SLJ13133	*MATa nbp1Δ::NATMX trp1::nbp1ΔAH-TRP1 his3-11,15::pRG203MX-nbp1ΔAH pURA3-ADE3-NBP1*	5B